engineering proceedings

MDPI

Proceeding Paper

Training MobileNet CNN for Simultaneous Sensing of Temperature and Bending Using Experimental Fiber Specklegrams †

Isaac Huertas-Montes [1,*], Francisco J. Vélez Hoyos [2,3] and Jorge Herrera-Ramírez [4]

[1] Faculty of Engineering, Institución Universitaria ITM, Medellín 050034, Colombia
[2] Faculty of Engineering, Universidad Cooperativa de Colombia (UCC), Medellín 050012, Colombia; francisco.velezh@campusucc.edu.co
[3] School of Applied Sciences and Engineering, EAFIT University, Medellín 050021, Colombia
[4] Faculty of Exact and Applied Sciences, Institución Universitaria ITM, Medellín 050034, Colombia; jorgeherrerar@itm.edu.co
* Correspondence: johnhuertas250382@correo.itm.edu.co
† Presented at the 13th International Electronic Conference on Sensors and Applications, 18–20 November 2026; Available online: https://sciforum.net/event/ECSA-13.

Abstract

Multimode optical fibers (MMFs) can be used as sensors due to their high sensitivity to chemical and physical perturbations, such as temperature and bending. It has been shown that, by training convolutional neural networks (CNNs) with the speckle patterns captured at the output of the sensing fiber, higher prediction accuracy for individual perturbations can be achieved compared to conventional methods as image correlation. In this work, a two-task CNN trained on experimental data is proposed to predict temperature and bending simultaneously. Data acquisition is automated via a MATLAB script controlling a contact heater for temperature and a linear displacement motor for inducing fiber bending through the displacement of one of its ends. Temperature varies from ~25 °C to 200 °C twice per linear translation stage across 5 fixed bending values or curvatures, producing 19,866 specklegram images acquired at the fiber output. For this work we adapted MobileNet CNN because of its lightweight architecture. The last dense layer has been modified to produce two outputs from a single specklegram: a continuous regression for temperature and a classification with five classes for bending, enabling the simultaneous sensing of both measurands through a single physical sensing mechanism, in contrast to conventional approaches that require multiple physical sensing methods or sensing elements. For evaluating the performance of the model, we calculate the coefficient of determination R^2 for linear temperature regression and classification accuracy for bending. The model achieves an R^2 of 0.9884 for temperature and an accuracy of 100% across the five bending classes. We found that most of the temperature error of the simultaneous model is a systematic offset that depends on the bending condition; excluding this offset, the estimated temperature resolution is about 4.4 °C, while bending is resolved down to the minimum spacing between classes (0.57 m^{-1}). These results show that the trained model can simultaneously estimate temperature (R^2 = 0.988) and classify the bending of a fiber sensor without errors from a single specklegram.

Keywords: fiber specklegram sensor; MobileNet architecture; temperature and bending

Check for updates

Academic Editor: Stefano Mariani

Published: 26 October 2026

Copyright: © 2026 by the authors. Licensee MDPI, Basel, Switzerland. This article is an open access article distributed under the terms and conditions of the Creative Commons Attribution (CC BY) license.

1. Introduction

Multimode optical fibers (MMFs) have been widely studied for sensing applications due to their sensitivity to external physical and chemical perturbations. Changes in param-

eters such as temperature [1,2], bending [3–5] or pressure [6] can modify the propagation conditions of the modes inside the fiber, resulting in changes in the intensity distribution observed at the fiber output [7,8]. The resulting interference pattern, commonly referred to as a speckle pattern or specklegram, contains information about the state of the fiber and can therefore be used as the sensing response.

Beyond their potential for laboratory-based measurements, fiber-optic sensors have demonstrated significant utility in practical applications where continuous, compact, and minimally intrusive sensing is required. In structural health monitoring, fiber-optic sensing technologies have been investigated for infrastructure such as bridges, pipelines, transportation systems, and other safety-critical structures, enabling the measurement of parameters such as strain and temperature and supporting tasks including damage detection, localization, and condition assessment [9]. Their immunity to electromagnetic interference, durability in harsh environments, and multiplexing capabilities further support their use in complex monitoring scenarios [9]. Similarly, in soft robotics, fiber-optic shape sensing has been used to obtain high-resolution information about the deformation and configuration of soft actuators, including their shape, twisting, and tip position, while also enabling the detection of contact and environmental features [10]. These applications illustrate the potential of fiber-optic sensing as a versatile platform for monitoring multiple physical conditions in systems where conventional electrical sensors or multiple sensing components may be difficult to integrate.

Several approaches have been proposed to extract information from fiber speckle patterns for the detection of physical perturbations [2,11]. Image-based methods combined with machine learning have demonstrated the ability to identify changes in the speckle pattern associated with specific perturbations [6,12,13]. Convolutional neural networks (CNNs) are particularly suitable for this task because they can automatically extract spatial features from images without requiring manual feature extraction [14,15]. Previous studies have shown that CNN-based models can achieve high prediction accuracy when trained to detect individual perturbations, such as temperature or bending, from speckle patterns acquired at the output of a multimode fiber [16]. However, when multiple perturbations are simultaneously applied to the fiber, the resulting speckle pattern is affected by the combined response of these parameters [17]. This introduces an additional challenge because the model must distinguish the contribution of each perturbation from a single optical response. Therefore, a model capable of learning the relationship between the speckle pattern and multiple physical parameters could provide a more suitable approach for simultaneous multiparameter sensing.

Multi-task learning provides a framework for addressing this problem by allowing a single neural network to perform multiple related tasks using a shared feature representation. In the context of fiber speckle sensing, as the specklegram serves as a multidimensional representation of the fiber's response, a multi-task CNN can extract common features from it while using separate output layers to estimate different physical parameters [4]. Such architecture avoids the need to develop a sensing method with a dedicated sensing element, measurement principle, or sensing configuration for each perturbation [17,18]. This approach can be used, for example, to perform continuous regression for temperature while simultaneously classifying discrete bending conditions

In addition to the sensing architecture, the practical implementation of the measurement system is an important consideration for generating the data required to train these models. Automated data acquisition can provide a controlled and repeatable procedure for applying temperature and bending perturbations while simultaneously recording the corresponding specklegrams [19]. This enables the generation of large datasets containing the optical response of the multimode fiber under different combinations of physical conditions.

https://doi.org/10.3390/engproc2026163007

In this work, a multi-task convolutional neural network trained with experimental specklegram data is proposed for the simultaneous detection of temperature over an extended range and several bending conditions in a multimode optical fiber. The data acquisition process is automated using MATLAB R2022a, which controls a heating block in contact with the fiber for temperature variation [19] and the linear translation stage motor for bending is controlled by the Thorlabs software Kinesis V1.14.59. Temperature is varied from 25~27 °C to 200 °C for five fixed bending conditions, generating 19,866 specklegram images at the output of the fiber. MobileNet architecture is adapted for this application due to its lightweight design, with the final layers modified to provide two outputs from a single specklegram: a continuous regression for temperature and a five-class classification for bending. The performance of the proposed approach is evaluated using numerical metrics as the Root Mean Squared Error (RMSE) and the coefficient of determination (R^2) for temperature estimation and classification accuracy for bending. The results demonstrate the capability of the proposed model to simultaneously estimate temperature and classify bending conditions from a single specklegram.

2. Methods

2.1. Experimental Data Acquisition

A sensing system was implemented to capture images of the speckle patterns when the optical fiber is perturbed. The experimental setup includes a light source (HeNe laser), a multimode optical fiber, a temperature and displacement control system, and a CMOS camera. Figure 1 shows the experimental setup.

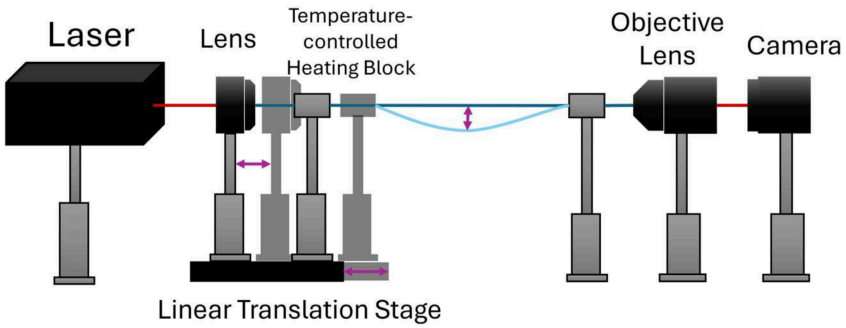


Figure 1. Schematic representation of the experimental setup. The red lines represent the laser light, the dark blue line represents the unbent fiber, and the light blue line represents the bent fiber. The purple arrows indicate the displacement of the translation stage and the resulting fiber bending.

The experimental setup comprises the following main components, which were selected to enable controlled application of the temperature and bending perturbations and the corresponding acquisition of the fiber specklegrams:

- Multimode optical fiber with a 25 μm core diameter and 62.5 μm cladding diameter.
- Arduino Mega 2560 for temperature control.
- RAMPS 1.4 board for power control.
- NTC 100 kΩ thermistor as the temperature sensor.
- 12 V, 40 W heating tube.
- 20X Olimpus microscope objective.
- Thorlabs USB 3.0 camera.
- 5 mm focal-length convex lens.
- 633 nm wavelength laser.
- Motorized translation stage with a Z925B servo motor and Thorlabs controller.

https://doi.org/10.3390/engproc2026163007

The fiber curvature can be calculated based on the horizontal displacement of one of the fiber ends using the formula shown in Equation (1).

$$c = \frac{1}{R} \cong \frac{1}{\sqrt{\frac{24d}{L_0^3}}}, \quad (1)$$

where L_0 is the length of the fiber curved zone (between the heating block and the fiber holder before the objective lens) with L_0 = 30 cm, and d is the horizontal displacement of one of the fiber ends. This allows us to have an approximate radius of the fiber's curvature based on the horizontal displacement [19].

2.1.1. Image Acquisition System

To register the changes in the specklegram pattern, images were captured with a CMOS camera, which is located at the end of the optical fiber. They were acquired automatically using a control system that synchronizes the image capture with the perturbations applied to the fiber. This allows us to get images with consequent values of temperature and curvature. The camera was programmed to take an image whenever a change of 0.175 °C occurs. These images are acquired after some stabilization time to guarantee that the fiber is in thermal equilibrium with the heating block.

2.1.2. Fiber Perturbations

To obtain the experimental data, the fiber was submitted to controlled perturbations of temperature and curvature. The multimode fiber was in contact with a temperature-controlled heating system consisting of a heating metal block, an electrical resistance, and a temperature sensor embedded in it. This way, the temperature could be measured in real time by a controller developed in Arduino integrated with MATLAB. The system is programmed to change the temperature with a resolution of 0.175 °C, waiting to assure temperature stabilization, and then going for the next step, changing temperatures from 25~27 °C to 200 °C up and down twice; this sequence was defined as one epoch.

For generating curvature perturbations, we used a linear translation stage with a servomotor and a Thorlabs controller giving a displacement resolution of 0.001 mm. For every temperature epoch, we moved the translation stage to four positions in 5 mm increments, i.e., from 0 mm to 20 mm, resulting in 5 curvature variations.

2.1.3. Dataset Building

In the MATLAB code, the images were named as shown in Figure 2, where every image is associated with its corresponding curvature and temperature value.

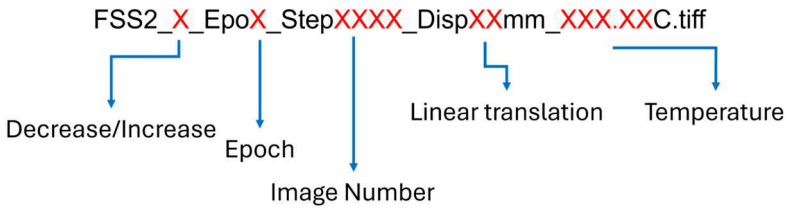


Figure 2. Image file naming convention.

When the temperature is rising or descending, this is labeled as Increase or Decrease; as the temperature goes from ~26 °C to 200 °C up and down twice, each cycle is an epoch, which is specified in the Epoch parameter (1 or 2). Every time the camera takes a photo, a number is assigned, this number is in the image file name next to Step. The linear translation is the distance of translation (0, 5, 10, 15 and 20). In this work, the

labels used for the bending condition correspond to these displacement values rather than directly to curvature or radius of curvature. However, based on the geometry of the experimental setup, these displacement conditions can be expressed in terms of equivalent radii of curvature of ∞, 47.43, 33.54, 27.38 and 23.71 cm (curvatures of 0, 2.11, 2.98, 3.65 and 4.22 m^{-1}) for displacements of 0, 5, 10, 15 and 20 mm, respectively. Finally, the temperature is the actual temperature of the fiber given by the temperature sensor.

This way, it is possible to determine the corresponding epoch of the image, and the temperature ramp direction.

2.2. CNN Training

The speckle images were used to train a model based on MobileNet Architecture, which has shown a high performance among different alternatives while being lightweight [20,21], allowing us to have a reference model for future applications in embedded systems. For this work, we trained three separate models to compare the effects of having two labels in the input data and two outputs to predict both perturbations simultaneously and separately. The characteristics of the models are shown in Table 1.

Table 1. Model architectures.

Parameter	Combined Model	Independent Temperature Model	Independent Curvature Model
Data labels	Curvature, Temperature	Temperature	Curvature
Transfer learning layers	2 Dense layers 1 Dropout layer 1 Curvature output branch 1 Temperature output branch	2 Dense layers 1 Dropout layer 1 Temperature output layer	2 Dense layers 1 Dropout layer 1 Curvature output layer
Output	Linear regression and Classification	Linear regression	Classification

2.3. Performance Metrics and Resolution

Temperature predictions were evaluated with the mean squared error (MSE), the root mean squared error (RMSE), the mean absolute error (MAE), the maximum absolute error and the coefficient of determination (R^2). For a test set of N samples with prediction error $e_i = T'_i - T_i$, the MSE can be split into two terms:

$$\mathrm{MSE} = \frac{1}{N}\sum {e_i}^2 = b^2 + \sigma^2, \tag{2}$$

where $b = \left(\frac{1}{N}\right)\sum e_i$ is the bias, or mean error, and $\sigma^2 = \left(\frac{1}{N}\right)\sum (e_i - b)^2$ is the variance of the error around that mean. Accordingly,

$$\mathrm{RMSE} = \sqrt{b^2 + \sigma^2}, \tag{3}$$

The bias describes a systematic offset that affects all readings in the same way and can be removed by calibration, while σ describes the random scatter that remains after such a correction. For this reason, the temperature resolution was estimated as

$$R_T = 2\sigma, \tag{4}$$

which corresponds to about 95% of the readings for normally distributed errors and, unlike 2·RMSE, does not include the correctable offset. Bending was treated as a five-class classification task and evaluated with the classification accuracy; its resolution was taken as the smallest curvature spacing between adjacent classes that the model distinguishes without error.

https://doi.org/10.3390/engproc2026163007

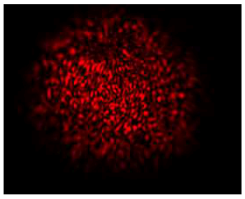
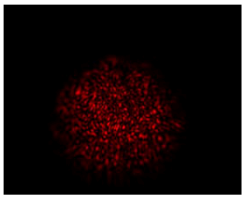
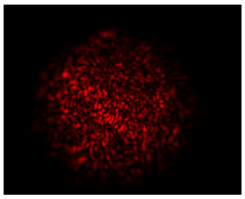
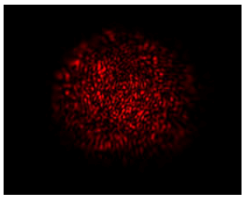
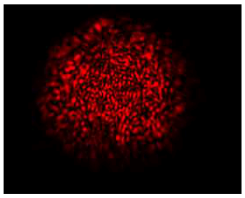
3. Results

3.1. Acquired Images

The experimental dataset was generated by applying five different bending conditions to the multimode optical fiber, corresponding to displacement values of 0, 5, 10, 15, and 20 mm. For each bending condition, the temperature varied from room temperature ~26 °C to 200 °C, while the corresponding specklegrams were continuously acquired at the fiber output.

A total of 19,866 specklegram images were obtained, corresponding to approximately 3973 images per bending condition. The number of images acquired for each condition is summarized in Table 2. The datasets corresponding to 0 and 20 mm contained 4001 and 4003 images, respectively, while the remaining three conditions contained 3954 images each. Therefore, the dataset is balanced across the five bending classes, with each class representing approximately 20% of the total dataset.

Table 2. Description of the experimental conditions and examples of captured specklegrams.

Displacement Value	Curvature	Specklegram	Temperature	# of Images	Temperature Range
0 mm	0 m^{-1}		25.45 °C	4001	25.45 °C to 200 °C
5 mm	2.11 m^{-1}		27.27 °C	3954	27.27 °C to 200 °C
10 mm	2.98 m^{-1}		27.27 °C	3954	27.27 °C to 200 °C
15 mm	3.65 m^{-1}		26.82 °C	3954	26.82 °C to 200 °C
20 mm	4.22 m^{-1}		25.45 °C	4003	25.45 °C to 200 °C

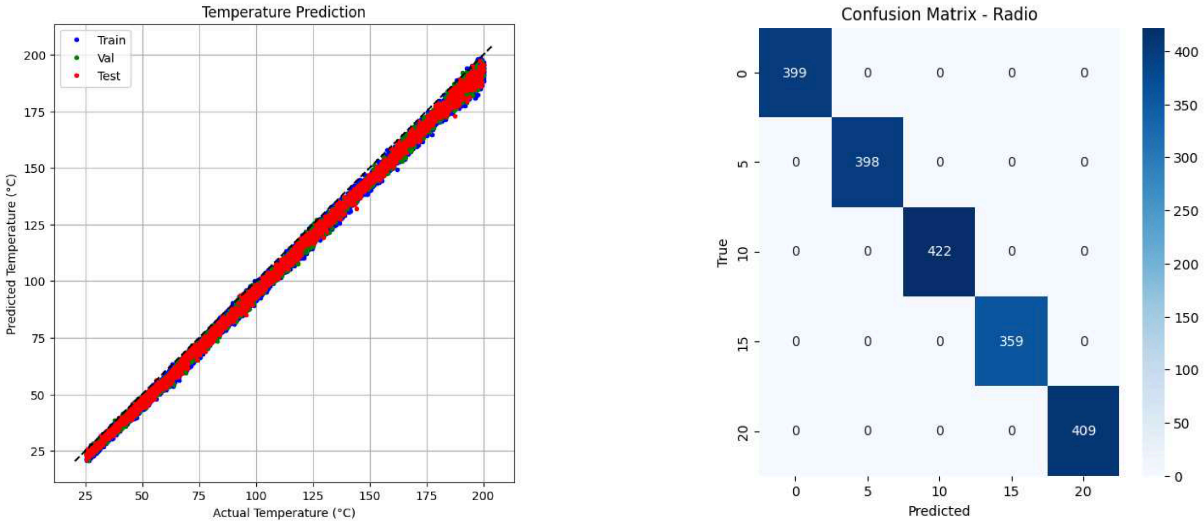
The initial temperature was not the same for all bending conditions due to variations in the laboratory environmental conditions and the initial state of the heating system. The first and last datasets started at approximately 25 °C, whereas the remaining datasets

started at approximately 27 °C. Nevertheless, all datasets covered a temperature range extending to approximately 175 °C, providing a broad range of thermal conditions for model training and evaluation.

Table 2 summarizes the experimental conditions and the number of specklegrams acquired for each bending value.

3.2. Simultaneous Temperature and Curvature Prediction

The performance of the proposed multi-task model is shown in Figure 3. The model receives a single specklegram as input and simultaneously produces two outputs: a continuous temperature estimation and a bending classification.

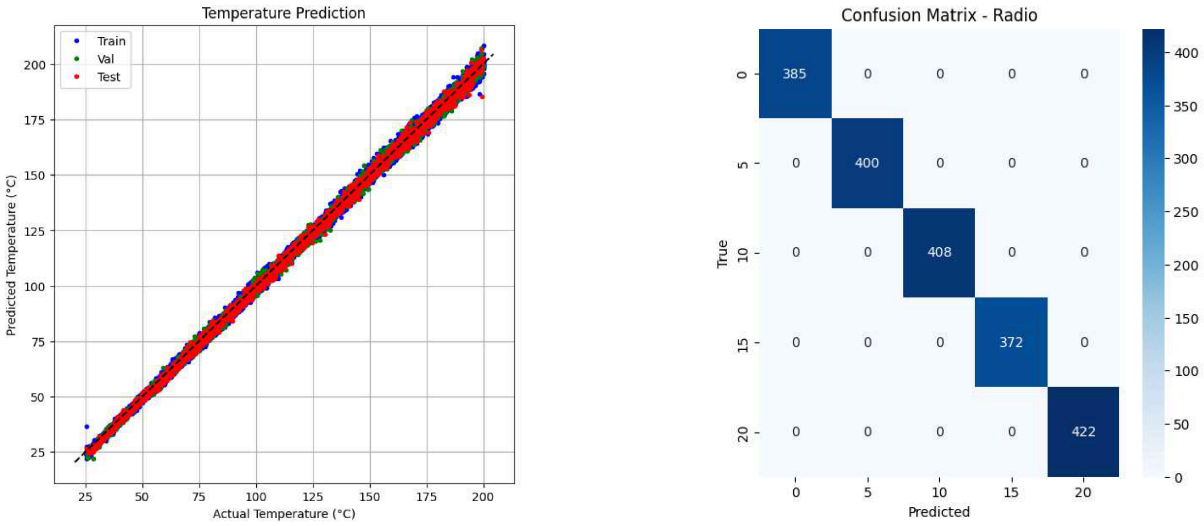


(**a**) (**b**)

Figure 3. Training results for the combined model. (**a**) Linear regression for the temperature output. (**b**) Confusion matrix for curvature classification.

Figure 3a shows the relationship between the measured and predicted temperature values for the test dataset. The predictions follow the general trend of experimental temperature values over the evaluated range. However, the model tends to underestimate the temperature, as can be seen by comparing Figure 3a with the independent model in Figure 4a. Almost all test points lie below the identity line, so the deviation behaves more like an offset than like random error. An offset of this kind could come from the experimental setup (for example, from the thermal contact between the fiber and the heating block), or from the model itself. As discussed in Section 4, the offset changes with the bending condition, which suggests that part of the bending effect is being read as a temperature change, and that it can be removed to a grand extent by a class-wise recalibration. Despite this deviation, the model maintains a strong correlation between the predicted and experimental values, resulting in an R^2 score of 0.9884.

The curvature classification results are presented in Figure 3b. The confusion matrix shows that all samples in the test dataset were correctly assigned to their corresponding bending class. No misclassified samples are observed for any of the five displacement conditions, resulting in a classification accuracy of 100%. This result indicates that the spatial features extracted from the specklegrams contain sufficient information to discriminate between the five bending conditions, even when the same feature representation is simultaneously used for temperature regression.



(**a**) (**b**)

Figure 4. Independent model results. (**a**) Linear regression of the model for temperature prediction. (**b**) Confusion matrix of the mode for curvature classification.

3.3. Independent Models

To evaluate the effect of performing both tasks simultaneously, independent models were trained separately for temperature prediction and curvature classification. The results are presented in Figure 4.

Figure 4a shows the regression results obtained using the independent temperature model. Compared with the simultaneous model, the predicted temperature values exhibit a closer fit to the experimental data. The independent model achieves an R^2 score of 0.9984, indicating a stronger agreement between the predicted and measured temperatures.

The independent curvature model also correctly classified all samples in the test dataset. As shown in Figure 4b, the confusion matrix contains no classification errors among the five bending classes, resulting in an accuracy of 100%. Therefore, both the simultaneous and independent approaches achieve the same classification performance for curvature.

3.4. Quantitative Comparison

The choice of performance metrics was determined by the nature of each prediction task and the architecture of the evaluated models. The temperature-related task is formulated as a continuous regression; therefore, MSE, MAE, RMSE, maximum error, R^2, bias and σ were calculated to quantify the magnitude and distribution of the prediction errors and the goodness of fit. Accuracy was not considered appropriate for temperature estimation because temperature is a continuous variable rather than a set of discrete classes. In contrast, bending is formulated as a five-class classification problem, for which accuracy provides a direct measure of the proportion of correctly classified bending conditions.

For the first model, which simultaneously performs temperature regression and bending classification through two output layers, the corresponding metrics for both tasks were calculated and reported. For the second and third models, which independently address a single sensing task, only the metrics corresponding to the task performed by each model were calculated. Therefore, regression metrics were reported for the temperature-only model, whereas accuracy was reported for the bending-only classification model. This metric selection ensures that each model is evaluated using measures appropriate to its specific prediction task.

The quantitative performance of the models is summarized in Table 3. The simultaneous model achieves an RMSE of 5.3977 °C and an R^2 score of 0.9884 for temperature prediction. For bending classification, the model achieves an accuracy of 100%.

Table 3. Model metrics.

Model	Simultaneous Model	Independent Temperature Model *	Independent Curvature Model **
MSE	29.1355	3.9438	NA
MAE	4.9249	1.5680	NA
RMSE	5.3977	1.9859	NA
Maximum	15.9115	12.7614	NA
R^2 score	0.9884	0.9984	NA
Bias	−4.9200	−0.7760	NA
σ	2.2200	1.8280	NA
Accuracy	1	NA	1

* In the temperature model, the Accuracy metric is not calculated; ** in the curvature model, the only metric calculated is the Accuracy.

In comparison, the independent temperature model provides lower regression errors, with an RMSE of 1.9859 °C, and an R^2 score of 0.9984. The MAE is approximately 86% lower than that of the simultaneous model, while the RMSE is approximately 63% lower. Similarly, the MSE is approximately 68% lower for the independent model. These results confirm the visual differences observed between the regression plots in Figures 3a and 4a.

Using Equation (2), the MSE of the simultaneous model (29.14 °C^2) is dominated by the bias term (b^2 = 24.21 °C^2, 83%), with a smaller random component (σ^2 = 4.93 °C^2). In the independent temperature model, the bias accounts for only 15% of the MSE (b^2 = 0.60 °C^2, σ^2 = 3.34 °C^2).

For curvature classification, both approaches achieve an accuracy of 100%. This indicates that introducing the temperature regression task into the same network does not negatively affect the classification of the five bending conditions.

4. Discussion

Other works have similar approaches to this work, using transfer learning from a CNN architecture, allowing for a comparison using the metrics presented. Table 4 shows this comparison.

As shown in Table 4, models trained with simulated data achieved lower temperature prediction errors than those trained with experimental data. However, the results obtained in this work should be considered in the context of the simultaneous analysis of two different perturbations and the classification of the displacement applied to the fiber. The independent temperature model achieved an RMSE of 1.9859 °C, compared with 0.45 °C and 0.94 °C reported for the SE-ResNet and MobileNet models, respectively. Although the proposed model presents a higher temperature error that those reported for models trained with simulated data, such as the SE-ResNet and MobileNet models, which achieved RMSE values of 0.45 °C and 0.94 °C, respectively, the proposed approach addresses the additional challenge of simultaneously processing temperature and bending from the same experimental specklegram. These results demonstrate the feasibility of using a lightweight multi-task CNN to extract information from a single specklegram under simultaneous perturbations.

https://doi.org/10.3390/engproc2026163007

Table 4. Metrics comparison.

Model	Data Source	MSE	MAE	RMSE	Maximum Error	R^2 Score
Simultaneous model	Experimental	29.1355	4.9249	5.3977	15.9115	0.988400
Independent temperature Model	Experimental	3.9438	1.5680	1.9859	12.7614	0.998400
MobileNet [16]	Simulated	12.9000	3.0500	3.5900	10.3000	0.989385
VGG-Reg [2]	Simulated	2.0164	1.3100	1.4200	2.95	0.998000
Correlation coefficient [2]	Simulated	10.3041	2.4500	3.2100	9.0800	0.992000
SE-ResNet [3]	Simulated	0.2100	0.3700	0.4500	1.1500	-

Compared with previous studies on multimode fiber specklegram sensing for temperature and bending, the present work extends the experimentally investigated temperature range from ~26 to 200 °C, providing a broader operating range than the 0–120 °C range considered in previous work, where a nonlinear response of the speckle correlation was observed above 120 °C [3]. In addition, this study relies exclusively on experimentally acquired data for model development and validation, while simultaneously enabling the prediction of both temperature and fiber curvature from a single specklegram. Finally, the use of lightweight MobileNet architecture, instead of the deeper SE-ResNet employed in [3], provides a more compact deep-learning solution while maintaining the capability of performing simultaneous multiparameter sensing.

Regarding resolution, most of the temperature error of the simultaneous model comes from a systematic underestimation (bias = −4.92 °C, 83% of the MSE), while the random component is σ = 2.22 °C. In the independent model, the bias is much smaller (−0.78 °C, 15% of the MSE), but the random component can be considered close to the value of the simultaneous model with a value σ = 1.828 °C. In both cases there is a bias, which suggests that part of the bending effect is interpreted as a temperature change, especially when both tasks share the same representation. Because this offset changes with the bending class, it could in principle be removed by a class-wise recalibration, which would bring the resolution of the simultaneous model closer to that of the independent one. Even without this recalibration both models reach similar resolutions, 2σ = 4.4 °C (2.5% of the 174.6 °C range) for the simultaneous model and 2σ = 3.7 °C (2.1% of the 174.6 °C range) for the independent model. The multi-task formulation therefore affects accuracy rather than resolution.

For bending, the models achieved an accuracy of 1.00, all 3973 test samples were correctly classified by both models (95% lower confidence bound: 99.9%). Therefore, the system was able to reliably distinguish the experimentally defined bending conditions. However, classification accuracy alone does not establish a continuous bending resolution; the minimum distinguishable bending variation is constrained by the separation between the discrete bending conditions included in the dataset. So the demonstrated resolution is the smallest spacing between classes, 0.57 m^{-1} (15 to 20 mm); finer values cannot be claimed without testing intermediate curvatures.

Since the train–test partition was random, these values describe interpolation within the acquired temperature ramps. A more detailed analysis, including resolution across the temperature range, hysteresis, repeatability between acquisition cycles and a class-wise recalibration of the bending-dependent offset, will be presented in future work.

5. Conclusions

In this work, a multimode fiber specklegram sensor was used for the simultaneous detection for temperature and bending using a multi-task convolutional neural network. An experimental dataset of 19,866 specklegrams was generated by automatically varying the temperature from approximately 25~27 °C to 200 °C under five different bending

conditions. The data acquisition process was controlled through MATLAB using a contact heater and a linear displacement motor, allowing the optical response of the fiber to be recorded under combined perturbations. A lightweight MobileNet architecture was adapted to process each specklegram and provide two outputs: temperature regression and bending classification.

The proposed model achieved an R^2 score of 0.9884 for temperature estimation and 100% accuracy for the classification of the five bending conditions. Although the independent temperature model achieved lower prediction errors, R^2 score of 0.9984 and an RMSE of 1.9859 °C, the simultaneous model successfully performed both sensing tasks from a single specklegram. The lower errors of the independent model come mainly from a systematic offset that depends on the bending in the simultaneous model, which accounts for 83% of its MSE. Excluding this offset, the estimated temperature resolutions (2σ) are 4.4 °C and 3.7 °C for the simultaneous and independent models, respectively, showing a closer performance than the RMSE values suggest. The bending resolution corresponds to the smallest spacing between classes, 0.57 m^{-1}.

Overall, the results show that the multi-task approach can successfully extract sufficient information from the specklegram images of a fiber with two different perturbations using a single lightweight neural network. A smaller offset dependent of the bending is also present in the independent temperature model, which suggests that the specklegram itself carries some cross sensitivity between both perturbations, and that sharing the feature representation between the two tasks makes it considerably stronger, so that part of the bending effect is read as a temperature change. Future work will therefore address a class-wise recalibration of this offset, as well as changes to the multi-task architecture and training strategy that reduce the interference between tasks while keeping the observed bending classification performance. A continuous estimation of curvature through regression, instead of classification, is also proposed, which would allow the bending resolution to be assessed beyond the spacing between the current classes.

Author Contributions: Conceptualization, J.H.-R. and F.J.V.H.; methodology, J.H.-R. and F.J.V.H.; software, I.H.-M.; validation, I.H.-M., J.H.-R. and F.J.V.H.; formal analysis, J.H.-R. and F.J.V.H.; investigation, I.H.-M., J.H.-R. and F.J.V.H.; resources, F.J.V.H. and J.H.-R.; data curation, I.H.-M.; writing—original draft preparation, I.H.-M.; writing—review and editing, J.H.-R. and F.J.V.H.; supervision, J.H.-R. and F.J.V.H. All authors have read and agreed to the published version of the manuscript.

Funding: This work was partially funded by Universidad Cooperativa de Colombia (UCC) (INV3612); Institución Universitaria ITM (PE24201), EAFIT University and MINCIENCIAS National Doctorates program.

Institutional Review Board Statement: Not applicable.

Informed Consent Statement: Not applicable.

Data Availability Statement: The raw data supporting the conclusions of this article will be made available by the authors on request.

Acknowledgments: During the preparation of this manuscript/study, the authors used OpenAI's ChatGPT (GPT-5.6 Luna) for the purposes of language translation and scientific writing refinement. The authors have reviewed and edited the output and take full responsibility for the content of this publication.

Conflicts of Interest: The authors declare no conflict of interest.

Abbreviations

The following abbreviations are used in this manuscript:

CNN	Convolutional Neural Network
RMSE	Root Mean Squared Error
MAE	Mean Absolute Error
MSE	Mean Squared Error

References

1. Yue, S.; Lu, H.; Li, B.; Che, Z. Feasibility of a Specklegram-Based Quasi-Distributed Temperature Sensor With Principal Component Analysis and Variational Autoencoder. *IEEE Sens. J.* **2024**, *24*, 22410–22418. [CrossRef]
2. Vélez, F.J.; Arango, J.D.; Aristizábal, V.H.; Trujillo, C.A.; Herrera-Ramírez, J. Comparative performance evaluation of classical methods and a deep learning approach for temperature prediction in fiber optic specklegram sensors. *Comput. Opt.* **2024**, *48*, 689–695. [CrossRef]
3. Liu, J.; Ke, Y.; Yang, D.; Deng, Q.; Hei, C.; Han, H.; Peng, D.; Wen, F.; Feng, A.; Zhao, X. Deep Learning-Based Simultaneous Temperature- and Curvature-Sensitive Scatterplot Recognition. *Sensors* **2024**, *24*, 4409. [CrossRef]
4. He, L.; Chen, X.; Cheng, J.; Yu, Y.; Liu, X.; Xu, L. Simultaneous measurement of displacement and torsion in a fiber specklegram sensor. *Opt. Lett.* **2026**, *51*, 3008–3011. [CrossRef]
5. Yuan, H.; Liu, Y.; Li, G.; Pang, L.; Yang, Z.; Cai, Y.; Wang, M. Torsion and bending sensing based on the specklegrams from a coupled few-mode multi-core fiber. *Opt. Commun.* **2024**, *569*, 130732. [CrossRef]
6. Reja, M.I.; Smith, D.L.; Viet Nguyen, L.; Ebendorff-Heidepriem, H.; Warren-Smith, S.C. Multimode Optical Fiber Specklegram Pressure Sensor Using Deep Learning. *IEEE Trans. Instrum. Meas.* **2024**, *73*, 1–10. [CrossRef]
7. Fujiwara, E.; Wu, Y.T.; Cordeiro, C.M.B. Entropy analysis of optical fiber specklegram sensors. *Results Opt.* **2021**, *5*, 100155. [CrossRef]
8. Lomer, M. Fenómeno speckle en fibra ópticas y sus aplicaciones en sensores. *TECNIA* **2012**, *22*, 5–16. [CrossRef]
9. Mahmood, Y.; Yasir, N.; Quenette, K.; Badin, G.; Huang, Y.; Xu, L. Fiber-Optic Sensor-Based Structural Health Monitoring with Machine Learning: A Task-Oriented and Cross-Domain Review. *Sensors* **2026**, *26*, 2641. [CrossRef]
10. Galloway, K.C.; Chen, Y.; Templeton, E.; Rife, B.; Godage, I.S.; Barth, E.J. Fiber Optic Shape Sensing for Soft Robotics. *Soft Robot.* **2019**, *6*, 671–684. [CrossRef]
11. Newaz, A.; Faruque, M.O.; Al Mahmud, R.; Sagor, R.H.; Khan, M.Z.M. Machine-Learning-Enabled Multimode Fiber Specklegram Sensors: A Review. *IEEE Sens. J.* **2023**, *23*, 20937–20950. [CrossRef]
12. Zhao, H.; Zhang, H.; Shen, D.; Zhang, L.; Qian, Z.; Zhang, A.D. Torsional sensing dataset based on multimode fiber scatterplot and its deep learning demodulation approach. *Laser Phys.* **2025**, *35*, 095101. [CrossRef]
13. Vélez H, F.J.; Arango, J.D.; Aristizábal-Tique, V.H.; Trujillo, C.; Herrera-Ramirez, J. Deep Learning-Based Method with Simulated Specklegrams for Temperature Prediction in a Fiber Specklegram Sensor. Available online: https://papers.ssrn.com/sol3/papers.cfm?abstract_id=4596616 (accessed on 30 November 2025). [CrossRef]
14. Inalegwu, O.C.; Roman, M.; Mumtaz, F.; Zhang, B.; Nambisan, A.; Huang, J. Machine learning-assisted optical fiber specklegram sensor for early and spatially distributed water leak detection and localization. *Opt. Eng.* **2025**, *64*, 1–26. [CrossRef]
15. Vélez Hoyos, F.J.; Arango, J.D.; Aristizábal, V.H.; Trujillo, C.; Herrera-Ramírez, J.A. Enhancing Temperature Sensing in Fiber Specklegram Sensors Using Multi-Dataset Deep Learning Models: Data Scaling Analysis. *Photonics* **2026**, *13*, 84. [CrossRef]
16. Huertas-Montes, I.; Vélez, F.; Aristizabal, V.; Trujillo, C.; Herrera-Ramírez, J. Evaluating the generalization capability of MobileNet-based CNNs for temperature prediction in simulated specklegram fiber optic sensors with combined synthetic. *Trans. Energy Syst. Eng. Appl.* **2025**, *6*, 1–12. [CrossRef]
17. Ming, Z.; Yubin, G.; Xiaosu, Z.; Tianshu, W.; Xuanguo, S. Study of cross-sensitivity in the fiber-optic sensor based on pervasive computing. In *Proceedings of the SPCA 2006: 2006 First International Symposium on Pervasive Computing and Applications*; IEEE: New York, NY, USA, 2006; pp. 797–801. [CrossRef]
18. Álvarez-Tamayo, R.I.; Durán-Sánchez, M.; Prieto-Cortés, P.; Salceda-Delgado, G.; Castillo-Guzmán, A.A.; Selvas-Aguilar, R.; Ibarra-Escamilla, B.; Kuzin, E.A. All-Fiber Laser Curvature Sensor Using an In-Fiber Modal Interferometer Based on a Double Clad Fiber and a Multimode Fiber Structure. *Sensors* **2017**, *17*, 2744. [CrossRef]
19. Vélez, F.J.; Arango, J.D.; Aristizábal, V.H.; Trujillo, C.; Herrera-Ramírez, J.A. Experimental Dataset for Fiber Optic Specklegram Sensing Under Thermal Conditions and Use in a Deep Learning Interrogation Scheme. *Data* **2025**, *10*, 44. [CrossRef]

20. David, J.; Moreno, A. Evaluación del uso de técnicas de Machine Learning para el análisis de patrones de interferencia modal en sensores de specklegramas de fibra óptica. 2023. Available online: https://hdl.handle.net/20.500.12622/6034 (accessed on 29 November 2025).
21. Howard, A.G.; Zhu, M.; Chen, B.; Kalenichenko, D.; Wang, W.; Weyand, T.; Andreetto, M.; Adam, H. MobileNets: Efficient Convolutional Neural Networks for Mobile Vision Applications. *arXiv* **2017**, arXiv:1704.04861. [CrossRef]

Disclaimer/Publisher's Note: The statements, opinions and data contained in all publications are solely those of the individual author(s) and contributor(s) and not of MDPI and/or the editor(s). MDPI and/or the editor(s) disclaim responsibility for any injury to people or property resulting from any ideas, methods, instructions or products referred to in the content.